Mode structure of a semiconductor laser subject to filtered optical feedback

Kirk Green and Bernd Krauskopf

Department of Engineering Mathematics
and Bristol Laboratory for Advanced Dynamics Engineering,
University of Bristol, Bristol BS8 1TR, UK

May 2005

Abstract

We present an analytical study of the mode structure of a semiconductor laser subject to filtered optical feedback (FOF). First, we derive expressions for the solution sets that define the structure of the modes. We then employ continuation techniques to investigate how this structure changes as filter width, filter detuning and feedback phase are varied. This leads to a comprehensive picture of the FOF laser's mode structure. In particular, we find an equation for the boundary of the parameter region in which one finds two separate components of modes.

Key words: Semiconductor laser, numerical continuation, singularity, delay differential equation

1 Introduction

The object of our study is a semiconductor laser subject to filtered optical feedback (FOF). As the name suggests, this type of feedback is different from conventional optical feedback (COF) due to the filtering of the laser's light. This filtering can be achieved in a number of different ways. For example, reflection from vapour cells or diffraction gratings naturally lead to filtering of the laser light [14]. Mutually coupled or compound lasers may also have a strong element of filtering, depending on the operating conditions [21]. Furthermore, a medium such as a Fabry-Perot interferometer can be placed inside the external cavity to produce filtered light [7]. The basic idea behind using FOF in applications is the possibility to control the laser's output. In particular, filtering can be used to obtain single-mode operation, or to select a specific frequency of the laser light [25]. Therefore, it is important to understand what

effect FOF has on the dynamics and mode structure of a laser in order to ensure desired operation.

The FOF laser can be modelled by rate equations that are similar to those derived by Lang and Kobayashi [18] for the COF laser; see Sec. 2 for details. An important element of this model is the time delay that arises due to the propagation time of the light in the external cavity prior to reentering the laser in filtered form.

The dynamics of the FOF laser (steady state operation, periodic oscillations and chaotic dynamics) have been investigated using numerical integration of the governing rate equations in a series of papers by Yousefi et al. Reference [27] identifies the steady states of the FOF laser with root finding techniques and then shows that the filter suppresses the well-known Sisyphus dynamic of the COF laser [22]. Reference [7] presents experimental results, which show good agreement with the numerical simulations. The influence of quantum noise on the dynamics of the FOF laser is investigated in Ref. [28]. The well-known low frequency fluctuations dynamic are identified for intermediate filter widths in Ref. [8]. An overview of the FOF laser can be found in Ref. [19]. Recently, an asymptotic investigation of the injection laser limit of the FOF laser was presented in Ref. [6]. This limit is also investigated in Ref. [13]. These studies have clearly demonstrated the richness of the dynamics of the FOF laser.

In this paper we perform a detailed analysis of the *external filter modes* (EFMs). These are the steady state solutions of the FOF laser. While forming the 'backbone' of the dynamics of the system, an analysis of this basic mode structure has been absent from the literature [1]. We derive analytical, transcendental expressions describing the EFM structure. Moreover, rather than using root finding, we employ the technique of numerical continuation to analyse these equations. This approach allows us to find and follow different branches of EFMs, so that we can examine how the solution structure changes as key parameters are varied. Specifically, we study how the EFM structure depends on the filter width Λ, the filter detuning Δ (with respect to the frequency of the free-running, fixed laser) and the feedback phase C_p of the external round-trip. These three parameters determine the external influence given by the filtered feedback on the otherwise fixed laser. Note that the feedback phase is an important physical parameter because changing it, for example, by changing the length of the external cavity on the order of a wavelength, may induce a switch from one EFM to another.

Our results give a comprehensive picture of the EFM structure that underlies the dynamics of the FOF laser. We give a geometric view of the influence of

[1] We remark that Matthias Wolfrum has independently obtained (unpublished) results on the mode structure.

the filter parameters Λ and Δ. Furthermore, we calculate the boundary that divides the (Λ, Δ)-plane into regions where the EFMs travel over a single or over two separate connected components as a function of C_p. The transitions between these two case are identified as passages through saddles and extrema in the surface of EFMs. Finally, we briefly discuss the limits for large and small filter width, which 'reduce' the system to a COF laser and an optically injected laser, respectively.

The study is organised as follows. In Sec. 2 we introduce the rate equations describing the FOF laser. The structure of the EFMs is studied analytically in Sec. 3. Continuation techniques are employed in Secs. 3.1 and 3.2 to investigate how the EFM structure changes as parameters are varied. The limits for large and small filter width are the topic of Sec. 4. Finally, in Sec. 5 we draw some conclusions and point to future work. A short appendix explains how one obtains the non-dimensionalised equations.

2 Rate equations for filtered optical feedback

A semiconductor laser subject to optical feedback can be described by the dimensionless rate equations [18]:

$$\frac{dE}{dt} = (1 + i\alpha)N(t)E(t) + \kappa F(t, \tau), \tag{1}$$

$$T\frac{dN}{dt} = P - N(t) - (1 + 2N(t))|E(t)|^2, \tag{2}$$

for the evolution of the complex electric field $E(t) = E_x(t) + iE_y(t)$ and the population inversion $N(t)$. Dimensionless parameters are the linewidth enhancement factor α, the ratio between the carrier lifetime and the photon decay rate T, and the rescaled pump rate P, which we fix at $\alpha = 5$, $T = 392.7$, and $P = 0.185$, respectively. These correspond to physical values of the carrier lifetime $\tau_e = 1.1 \times 10^{-9}$ s, the photon decay rate $\tau_p = 3.57 \times 10^{11}$ s^{-1}, and a normalised pump rate $J = 1.5\, J_{\text{th}} = 1.40 \times 10^{17}$ s^{-1}; the full physical model is detailed in the Appendix.

The feedback term $\kappa F(t, \tau)$ in Eq. (1) involves the dimensionless feedback rate $\kappa = 4.12045 \times 10^{-2}$, corresponding to a physical feedback rate of 14.71 GHz [26], and the dimensionless propagation time between the laser and the external reflector $\tau = 357$, corresponding to a physical distance of $L_{\text{ext}} \approx 15$ cm.

For the case of a semiconductor laser subject to conventional optical feedback (COF), the feedback function in Eq. (1) reduces to $F(t, \tau) = E(t - \tau)$. In

this paper, we consider filtered optical feedback (FOF) modelled by a single-Lorentzian approximation as [27]

$$F(t,\tau) = \Lambda e^{i(C_p - \Omega\tau)} \int_{-\infty}^{t} E(s-\tau) \exp\left[(i(\Delta-\Omega)-\Lambda)\, s\right] ds\,.$$

Rather than using this integral function in conjunction with Eqs. (1)–(2) it is better to differentiate it with respect to time to obtain the dimensionless differential equation

$$\frac{dF}{dt} = \Lambda E(t-\tau) e^{i(C_p - \Omega\tau)} + (i(\Delta-\Omega)-\Lambda)\, F(t) \tag{3}$$

for the complex feedback field $F(t) = F_x(t) + iF_y(t)$.

Equations (1)–(3) are written in the frame of reference of the solitary laser at some fixed experimental conditions, in particular, constant pump current and constant temperature. The parameter Ω measures the detuning of the free-running frequency of the laser with respect to the fixed frequency. In other words, the situation that $\Omega = 0$ corresponds to the experimental setup where the laser parameters are kept fixed at all times. In this case, the detuning between the laser and the filter is given by Δ. Alternatively, one can fix Δ, that is, the detuning of the filter with respect to the reference frequency. The detuning parameter between the laser and the mirror in this case is $\Delta - \Omega$, so that the detuning is effected by changing the free-running laser frequency by Ω (for example by small changes of temperature or pump current). Note that this changes the feedback phase term $e^{i(C_p - \Omega\tau)}$.

In this paper we think of the laser as fixed, that is $\Omega = 0$, so that the main parameters describe the effect of the filtered field that is fed back into the laser. These are the filter detuning Δ, the filter width Λ, the feedback strength κ, and the feedback phase C_p. Note that C_p is an independent parameter (it does not depend of Δ) that can be controlled experimentally, for example, by using a piezoelectric actuator to vary the distance between the laser and the external reflector on the scale of the optical wavelength ($\sim O(10^3)$ nm) [12]. In our analysis we assume that changing C_p on this scale has no effect on the value of τ, which is typically on the order of centimetres. This point of view leads to simpler mathematical formulas and has advantages in the numerical continuation of EFMs, which in this framework are intersections of solution loci with the fixed line $\Omega = 0$.

Mathematically, Eqs. (1)–(3) form a system of delay differential equations (DDEs) with a single fixed delay τ. The phase space of Eqs. (1)–(3) is the infinite-dimensional space of continuous functions over the interval $[-\tau, 0]$ with values in $\mathbb{R}^5$, namely in (E, N, F)-space. For further reading on DDEs

see Refs. [3,11,15]. Furthermore, Eqs. (1)–(3) are invariant under the transformation

$$(E, N, F) \to (cE, N, cF), \tag{4}$$

where $\{c \in \mathbb{C} \,|\, |c| = 1\}$ [17]. One speaks of a continuous S^1-symmetry: rotating any solution in the complex E and F planes over any angle $b \in [0, 2\pi]$ yields another solution of Eqs. (1)–(3). This symmetry property is shared with the Lang-Kobayashi equations describing the COF laser. Note that in Eq. (3), as the filter width $\Lambda \to \infty$, we recover the equation for COF because $F(t, \tau) \to E(t - \tau)$; see also Sec. 4.

An interesting observation is that Eqs. (1)–(3) are quite similar in structure to the rate equations describing a semiconductor laser subject to non-instantaneous phase-conjugate feedback (PCF) [2,10]. Specifically, the inverse Λ^{-1} of the filter width of the FOF laser plays a similar role to the propagation time t_m within the phase-conjugate mirror (PCM). The main difference between Eqs. (1)–(3) and those for the PCF laser is the conjugation of the electric field after reflection from the PCM. This changes the symmetry properties of the governing system. The rate equations for the FOF laser (and the COF laser) have the continuous S^1-symmetry (4), whilst the rate equations for the PCF laser have a discrete $\mathbb{Z}_2$-symmetry [9,17].

3 External filtered modes

In analogy with the external cavity modes (ECMs) of the COF laser, we call the basic steady state solutions of Eqs. (1)–(3) *external filtered modes* (EFMs). They are of the form

$$(E(t), N(t), F(t)) = (E_s e^{i(\omega_s - \Omega)t},\ N_s,\ F_s e^{i(\omega_s - \Omega)t + i\Phi}) \tag{5}$$

where $E_s, N_s, F_s, \omega_s, \Phi \in \mathbb{R}$. Specifically, ω_s is the frequency mismatch from the solitary laser frequency. Physically, EFMs are frequency locked solutions, operating at a constant amplitude and at a constant inversion. As for the COF laser, this ansatz is motivated by the S^1-symmetry (4). Inserting it into Eqs. (1)–(3) results in the equation

$$\Omega = \omega_s + \kappa\Lambda \sqrt{\frac{1 + \alpha^2}{\Lambda^2 + (\Delta - \omega_s)^2}} \sin\left(-\Phi + \arctan\alpha\right) \tag{6}$$

where

$$\Phi = C_p - \omega_s \tau - \arctan\left(\frac{\Delta - \omega_s}{\Lambda}\right). \tag{7}$$

Equations (6)–(7) provide solutions for ω_s which are given by a sinusoidally varying function, off-set by Ω. Importantly, the amplitude of the sinusoidal function depends on the filter parameters in a non-trivial way; the amplitude is independent of the feedback phase C_p. We study this dependency in detail in Sec. 3.1. Once ω_s is known, the inversion, and the amplitudes of the electric field and the feedback field can then be found as

$$N_s = -\kappa \frac{\Lambda}{\sqrt{\Lambda^2 + (\Delta - \omega_s)^2}} \cos(\Phi), \tag{8}$$

$$E_s = \sqrt{\frac{P - N_s}{1 + 2N_s}}, \tag{9}$$

$$F_s = \frac{\Lambda E_s}{\sqrt{\Lambda^2 + (\Delta - \omega_s)^2}}. \tag{10}$$

The transcendental Eq. (6) for ω_s needs to be solved numerically. For this purpose we use the technique of numerical continuation to find and follow solutions of Eqs. (6)–(10) in relevant parameters. This method is ideally suited when calculating solution curves around fold points where straightforward root finding with, for example, Newton's method may have difficulties. Indeed, continuation techniques have been extremely valuable in understanding the dynamical structure of a number of laser systems; see, for example, the recent overviews [15,16]. Solutions of the transcendental system Eqs. (6)–(10) can be calculated with, for example, the numerical continuation package `AUTO` [4]. Here we use the `Matlab` package `DDE-BIFTOOL` [5]. Specifically, we use its pseudo-arclength continuation routines to find and follow solutions as parameters are varied. We remark that `DDE-BIFTOOL` has an advantage over `AUTO` in that it can also be used to obtain stability information of the full nonlinear DDEs Eqs. (1)–(3) describing the FOF laser. However, this is beyond the scope of this paper.

A typical *solution curve* of Eq. (6) is shown (in black) in Fig. 1. The solution curve is enclosed by a *solution envelope* (in grey). This is defined by the sine term of Eq. (6) taking its extreme values of ± 1, in other words, by

$$\Omega_e(\omega_s) = \omega_s \pm \kappa\Lambda \sqrt{\frac{1 + \alpha^2}{\Lambda^2 + (\Delta - \omega_s)^2}}. \tag{11}$$

Note that both the solution curve and (both branches of) the solution envelope are single-valued functions determining Ω as a function of ω_s. This is an

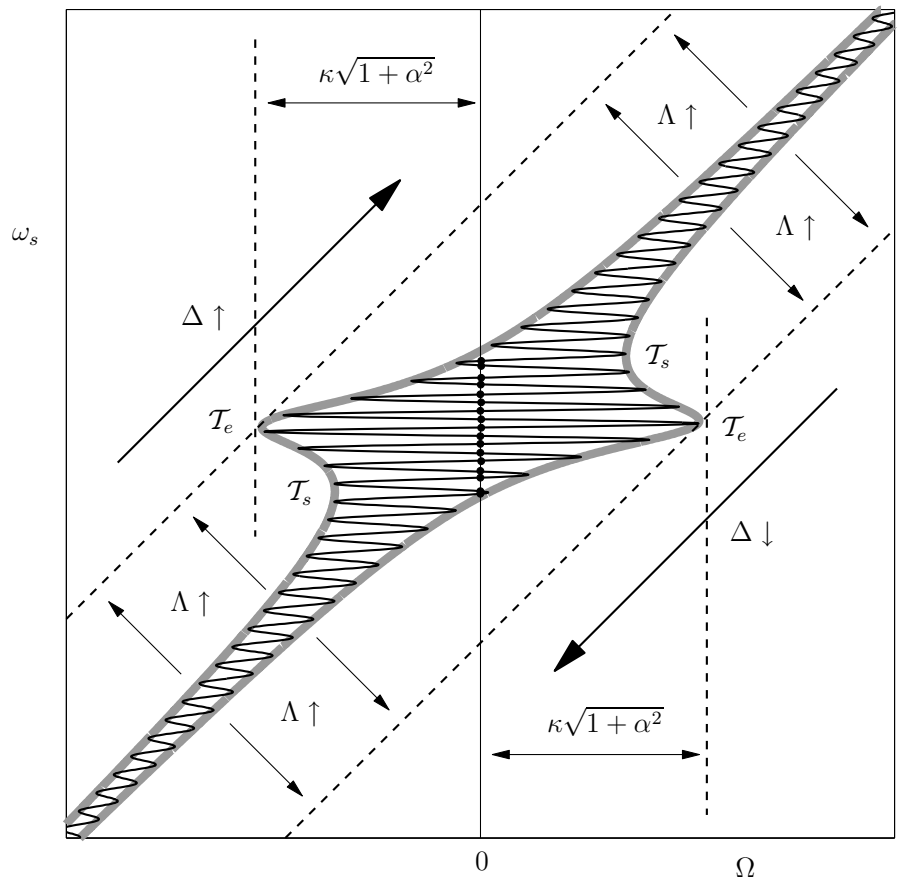

Fig. 1. Example of a solution curve and solution envelope; here $(\Lambda, \Delta) = (0.025, 0.0)$.

important realization for the mathematical analysis. The shape of the solution envelope is independent of the feedback phase C_p, with its width given by the effective feedback strength $\kappa\sqrt{1+\alpha^2}$. Note that when $\Omega_e = 0$ (the situation considered here) Eq. (11) is invariant under the symmetry operation

$$(\omega_s, \Delta) \mapsto (-\omega_s, -\Delta)\,,$$

so that we can restrict to the case of, say, positive Δ from now on. Changing the filter detuning Δ moves the solution curve, and the solution envelope, of Fig. 1 along the diagonal. Increasing the filter width Λ results in the envelope moving closer to the dashed curves

$$\Omega_e(\omega_s) = \omega_s \pm \kappa\sqrt{1+\alpha^2}. \tag{12}$$

In other words, as $\Lambda \to \infty$ we recover the constant sinusoidal curve describing the ECMs of the COF laser contained within an envelope of constant amplitude given by $\kappa\sqrt{1+\alpha^2}$; see already Sec. 4 and Fig. 8.

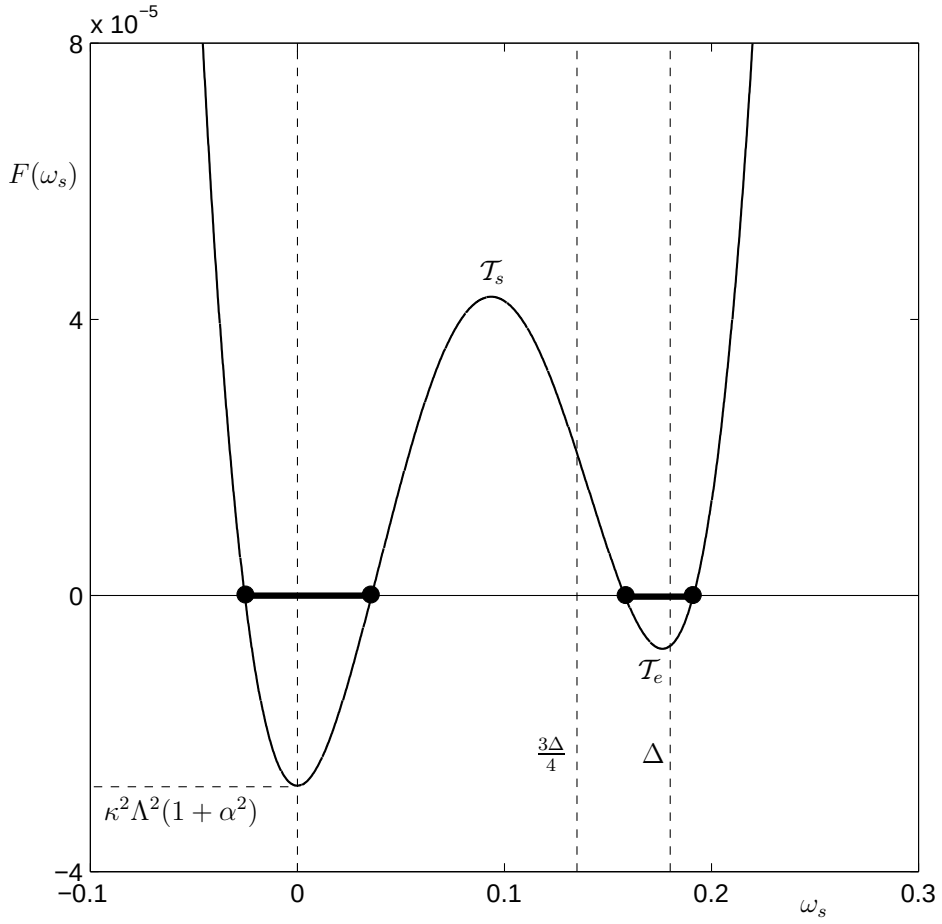

Fig. 2. Graph of the fourth-degree polynomial $F(\omega_s)$ of Eq. (13) for $\Delta = 0.180$, $\Lambda = 0.025$. The roots (dots) bound two intervals of ω_s values corresponding to two EFM-components (thick lines); one interval always contains $\omega_s = 0$ (the free running laser mode) and the second contains the filter frequency Δ.

For a fixed value of C_p the solution curve intersects the vertical line $\Omega = 0$ in a finite number of points, which are exactly the EFMs we want to find. As C_p is varied over 2π, the solution curve defined by Eq. (6) changes and actually fills the entire interior of the envelope. Furthermore, as C_p is changed, EFMs are created in mode/antimode pairs in saddle-node bifurcations. In projection onto the (ω_s, N_s)-plane the EFMs move, as a function of C_p, over a single or over two separate closed curves, which we call *EFM-components*. Note that the EFM-components are the counterpart of the well known ECM ellipse of the COF laser; see already Sec. 3.2 and Fig. 6. The shape of the EFM-component(s) depends only on the shape of the solution envelope, that is, only on Λ and Δ, and not on C_p.

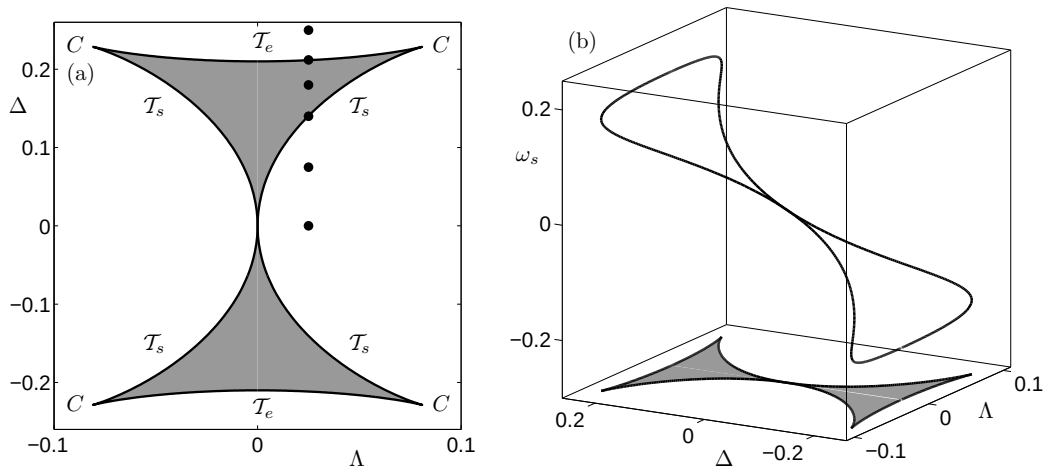

Fig. 3. Regions in the (Λ, Δ)-plane in which a single EFM-component (exterior of curve) and two isolated EFM-components (shaded region, interior of curve) exist. The black points in (a) correspond to the parameter values used in Figs. 5, 6 and 7. Panel (b) shows that the cusp points shown in panel (a) are the projection of a smooth curve in $(\Lambda, \Delta, \omega_s)$-space.

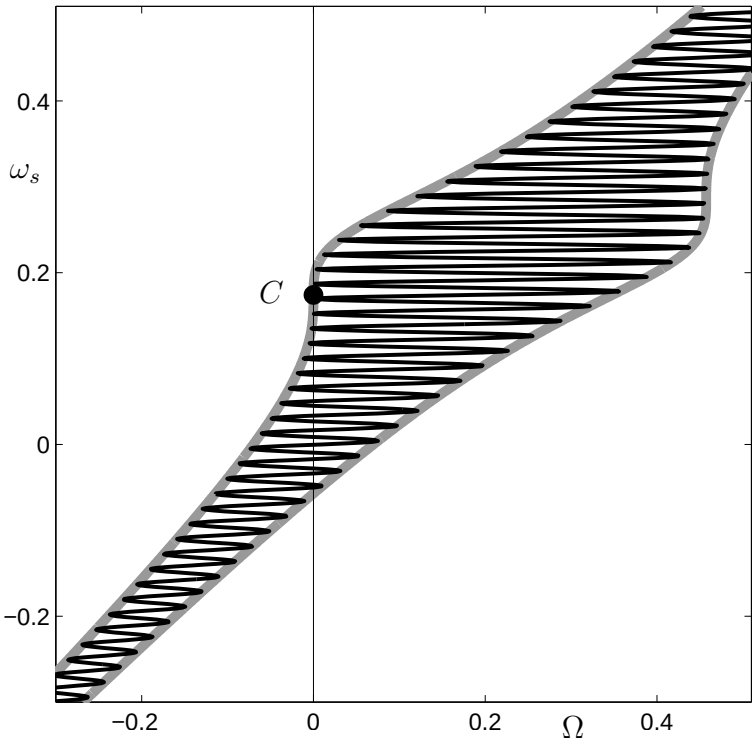

Fig. 4. Cusp point (cubic tangency with $\Omega = 0$) of the envelope for $(\Lambda, \Delta) = (0.081, 0.229)$.

The solution envelope in Fig. 1 has a 'bulge' centred around the detuning Δ of the filter. As Δ is varied this bulge moves along the diagonal. This has the consequence that for certain values of Λ and Δ one finds two rather than just one intersection of the line $\Omega = 0$ with the interior of the envelope. This can be studied by setting $\Omega_e(\omega_s) = 0$ in Eq. (11), which yields the ω_s values at the intersections of the envelope with $\Omega = 0$ as the roots of the fourth-order polynomial

$$F(\omega_s) = \omega_s^2 \left((\Delta - \omega_s)^2 + \Lambda^2 \right) - \kappa^2 \Lambda^2 \left(1 + \alpha^2 \right). \tag{13}$$

Moreover, these roots bound intervals of ω_s values that correspond to different EFM-components, so that the function $F(\omega_s)$ presents a geometrical interpretation of the EFM-components in dependence with Δ and Λ. Figure 2 shows the graph of $F(\omega_s)$ for the case that there are two EFM-components.

The number of EFM-components changes when fold points (with respect to Ω) of the envelope pass through the line $\Omega = 0$. This corresponds to a transition $\mathcal{T}_\mathrm{e}$ through an extremum or a transition $\mathcal{T}_\mathrm{s}$ through a saddle point of the associated surface of EFMs. These fold points are given by roots of the first derivative of Eq. (11) with respect to ω_s, that is, by

$$\begin{aligned} \frac{d\,\Omega_e}{d\,\omega_s} &= 1 \mp \kappa\Lambda \sqrt{\frac{1+\alpha^2}{\Lambda^2 + (\Delta - \omega_s)^2}} \left(\frac{\omega_s - \Delta}{\Lambda^2 + (\Delta - \omega_s)^2} \right) \\ &= 1 + \omega_s \left(\frac{\omega_s - \Delta}{\Lambda^2 + (\Delta - \omega_s)^2} \right) = 0\,, \end{aligned} \tag{14}$$

where we used Eq. (11) for $\Omega_e(\omega_s) = 0$. It can readily be seen that Eq. (14) is equivalent to

$$\frac{dF(\omega_s)}{d\omega_s} = 2\omega_s^2 - 3\Delta\omega_s + \Delta^2 + \Lambda^2 = 0, \tag{15}$$

from which we conclude that the fold points (the extrema of $F(\omega_s)$) are at

$$\omega_s = 0, \quad \text{and} \quad \omega_s = \frac{3\Delta \pm \sqrt{\Delta^2 - 8\Lambda^2}}{4}\,. \tag{16}$$

The extremum at $\omega_s = 0$ is always a minimum since $F(0) = -\kappa^2\Lambda^2\,(1+\alpha^2)$. The two folds for $\omega_s \neq 0$ exist only for $\Delta^2 \geq 8\Lambda^2$. The smaller one is a

maximum ($\mathcal{T}_\mathrm{s}$) and the larger one a minimum ($\mathcal{T}_\mathrm{e}$) (note that we consider $\Delta \geq 0$); see Fig. 2. These extrema coincide in the cusp point

$$\omega_s = \frac{3\Delta}{4} \quad \text{for} \quad \Delta^2 = 8\Lambda^2. \tag{17}$$

To check that we are indeed dealing with a cusp we consider

$$\frac{d^2\,\Omega_e}{d\,\omega_s^2} = \pm\kappa\Lambda\sqrt{\frac{1+\alpha^2}{\Lambda^2+(\Delta-\omega_s)^2}}\left\{\frac{2(\Delta-\omega_s)^2-\Lambda^2}{\left(\Lambda^2+(\Delta-\omega_s)^2\right)^2}\right\}. \tag{18}$$

It is easily verified that $\frac{d^2\,\Omega_e}{d\,\omega_s^2} = 0$ since $2(\Delta-\omega_s)^2-\Lambda^2 = 0$ at the cusp point given by Eq. (17). By using Eqs. (13) and (17) the cusp points are found at

$$(\Lambda,\Delta) = \left(\pm\frac{2}{3\sqrt{3}}\kappa\sqrt{1+\alpha^2}, \pm\frac{4\sqrt{2}}{3\sqrt{3}}\kappa\sqrt{1+\alpha^2}\right). \tag{19}$$

We find the locus of the passage through folds as the filter parameters Λ and Δ are varied by using the pseudo-arclength continuation routines of `DDE-BIFTOOL` [5] to simultaneously solve the implicit equations (11) and (14). Figure 3(a) shows the resulting curve in projection onto the (Λ,Δ)-plane. The interpretation of this result is as follows. In the region outside this curve one finds a single EFM-component, while inside the shaded region one finds two isolated EFM-components. The curves bounding the shaded region of Fig. 3 to the left and right correspond to saddle transitions $\mathcal{T}_\mathrm{s}$ of the envelope (with respect to $\Omega = 0$) and the curves at the top and bottom correspond to transitions through extrema $\mathcal{T}_\mathrm{e}$ of the envelope. The two curves $\mathcal{T}_\mathrm{s}$ and $\mathcal{T}_\mathrm{e}$ meet at cusp points C. Figure 3(b) shows that the solution of Eqs. (11) and (14) is a single smooth curve in in $(\Lambda,\Delta,\omega_s)$-space, which can be readily continued numerically. The turning points in this curve are the cusp points, with values satisfying Eq. (17).

The solution curve and corresponding envelope at this cusp point C for $(\Lambda,\Delta,\omega_s) = (0.081, 0.229, 0.172)$ is shown in Fig 4; compare already with Fig. 6. The envelope clearly has a cusp at $\Omega = 0$, marked by a point. Note that at the cusp point the third derivative of Eq. (11) with respect to ω_s must be non-zero, which is the case for $\Delta \neq \omega_s$ and $\kappa, \Lambda \neq 0$.

Finally, we note that the region shown in Fig. 3 scales linearly with the effective feedback strength $\kappa\sqrt{1+\alpha^2}$. In other words, the region retains its shape yet grows linearly with $\kappa\sqrt{1+\alpha^2}$; compare with Eq. (19).

3.2 Bifurcations of EFMs

We illustrate the connection between the solution curve and the bifurcations of EFMs with three figures. Figure 5 shows the solution curve (in black) defined by Eq. (6) and the corresponding solution envelope (in grey) defined by Eq. (11). Figures 6 and 7 show the results of continuing an EFM of the FOF laser as the 2π-periodic feedback phase C_p of Eq. (3) is varied. In other words, Figs. 6 and 7 show the EFM-components in different projections. The dots on the EFM-components in Fig. 6 are the EFMs for C_p=0. Figures 5–7 are for the fixed parameter values given in Sec. 2, plus a fixed filter width of $\Lambda = 0.025$, and, from panel (a) to (e) in each figure, a varying filter detuning of $\Delta = 0.0$, 0.075, 0.140, 0.180, 0.212, and 0.25. These values correspond to the black dots shown in the (Λ, Δ)-plane of Fig. 3.

As is the case for the COF laser, C_p parameterises the EFM-components on which the EFM steady state solutions exist. We remark that it has already been shown in Ref. [27] that the EFMs lie on closed curves or isolas — the EFM-components in our notation — but they have not been derived analytically or computed as continuous curves. We show the EFM-components in Fig. 6 in projection onto the (ω_s, N_s)-plane as computed with numerical continuation. (This projection is well known from illustration of the ECM ellipse of the COF laser.)

Figure 7, on the other hand, displays the same information, but 'unwrapped' in the (C_p, ω_s)-plane over a range of the 2π-periodic parameter C_p. In this case, the finite EFM solutions can be found by taking a vertical slice through Fig. 7 for a given value of C_p. The black dots in Fig. 5 correspond to the slice at $C_p = 0$.

We now come to a description of the transition of the EFM-components as the filter detuning Δ is varied. For $\Delta = 0$ the bulge of the solution envelope is centred at the origin of the (ω_s, Ω)-plane; see Fig. 5(a). The associated single EFM-component is shown in Fig. 6(a). It corresponds to the single, continuous curve in Fig. 7(a). As Δ is increased, the bulge in the envelope moves along the diagonal towards the top-right of the (ω_s, Ω)-plane; see Fig. 5(b). The EFM-component deforms in the (ω_s, N_s)-plane but it is still a single closed curve; see Figs. 6(b) and 7(b). It surrounds both the frequency of the filter $\omega_s = \Delta$ and the free-running laser frequency $\omega_s = \Omega = 0$.

As the filter detuning Δ is increased further, the envelope undergoes a saddle transition $\mathcal{T}_\mathrm{s}$ at $\Omega = 0$, which can be seen clearly in the Figs. 6(c) and 7(c) as a point where the curve self-intersects near $\omega_s = 0.1$. Past this saddle transition we now have two intersections with the interior of the envelope and there are now two EFM-components centred around $\omega_s = \Omega$ and $\omega_s = \Delta$, respectively;

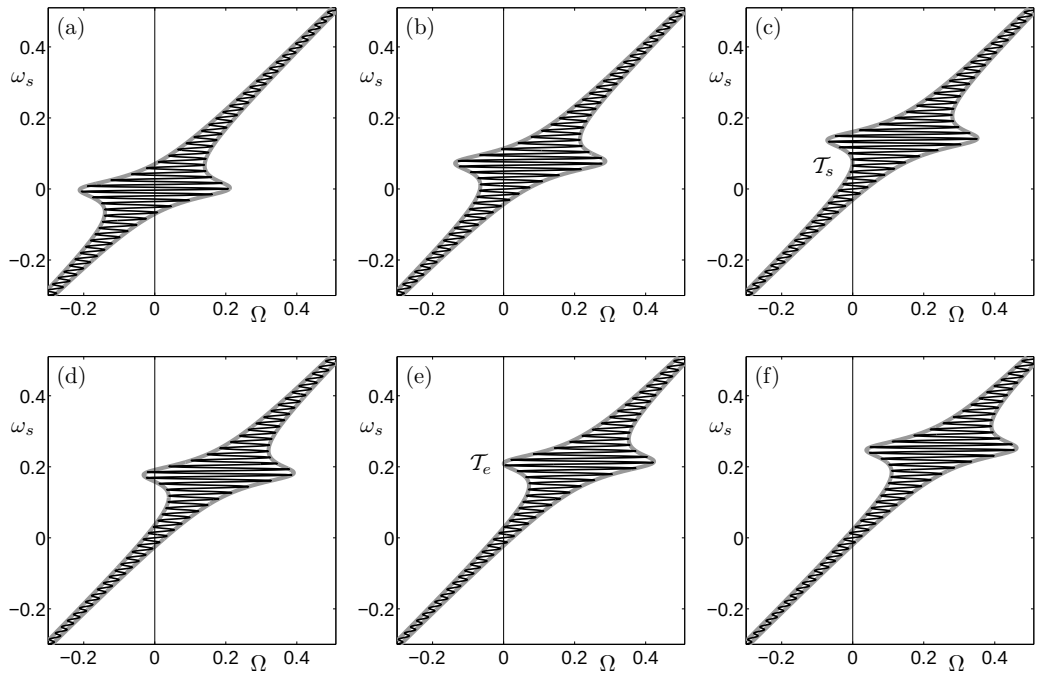

Fig. 5. Solution envelopes (in grey) and curves (in black) corresponding to the black dots in Fig. 3. Here $\Lambda = 0.025$ and from (a) to (f) the filter detuning was fixed at $\Delta = 0.0$, 0.075, 0.140, 0.180, 0.212, and 0.25.

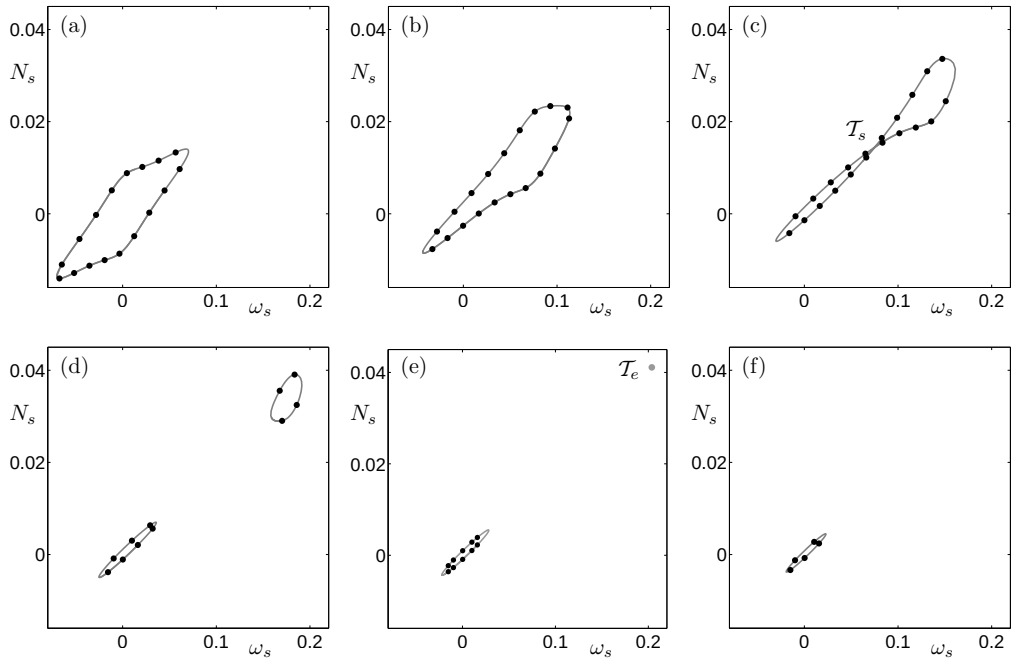

Fig. 6. Curves of EFMs in the (ω_s, N_s)-plane. The black dots correspond to a discrete set of EFMs for $C_p = 0$. Here $\Lambda = 0.025$ and from (a) to (f) the filter detuning was fixed at $\Delta = 0.0$, 0.075, 0.140, 0.180, 0.212, and 0.25.

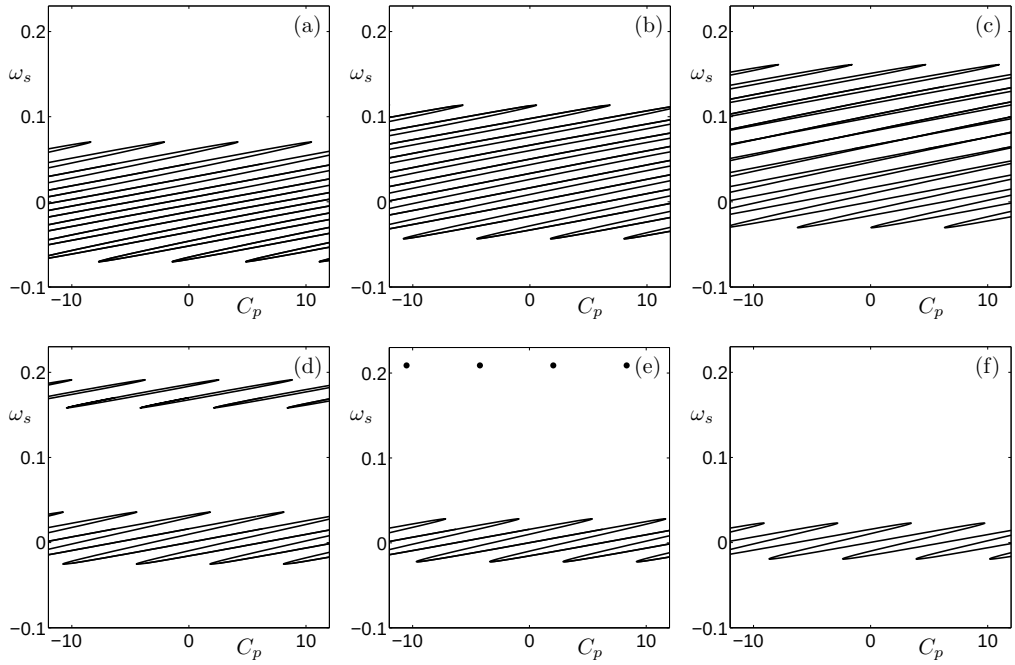

Fig. 7. Curves of EFMs in the (C_p, ω_s)-plane. These curves represent those shown in Fig. 6 'unwrapped' and plotted over a large range of C_p. Here $\Lambda = 0.025$ and from (a) to (f) the filter detuning was fixed at $\Delta = 0.0$, 0.075, 0.140, 0.180, 0.212, and 0.25, respectively.

see Figs. 6(d). In the (C_p, ω_s)-plane this corresponds to a continuous curve centred around $\omega_s = \Omega$ and infinitely-many unconnected closed curves centred around $\omega_s = \Delta$; see Fig. 7(d). This situation corresponds to the grey region in Fig. 3.

Increasing the filter detuning Δ further one crosses the curve $\mathcal{T}_\mathrm{e}$ of Fig. 3, passing from the two EFM-component region back into the outer, one EFM-component region. The envelope at the crossing point, $\Delta = 0.212$, is shown in Fig. 5(e) to undergo a transition through an extremum at $\Omega = 0$. At this point, the EFM-component centred around $\omega_s = \Delta$ shrinks to a point; see Fig. 6(e). For $C_p = 0$ there are no EFMs on the grey solution envelope (the point) in the top-right corner of Fig. 6(e). The only discrete number of EFMs on this part of the solution envelope occur for $C_p \approx 1.35\pi \pm 2m\pi$, $m \in \mathbb{N}$. This is confirmed in Fig. 7(e) were the infinitely-many closed curves are also shown to shrink to points. After this transition a single, small EFM-component, centred around $\omega_s = \Omega$, exists; see Figs. 4(f), 6(f) and 7(f). Physically, the filter is now detuned so far from the laser that the laser cannot sustain EFMs near the filter frequency Δ any longer.

We finally note that panels (a) and (f) in Figs. 6 and 7 are qualitatively the same. This corresponds to the fact that one can get from one situation to the other continuously, without crossing into the grey region in Fig. 3 by changing Δ and Λ appropriately.

4 Limits of large and small filter width

For any value in the white region of Fig. 3 there is a single EFM-component. This is qualitatively like the situation for the COF laser, but the ECM ellipse is deformed by the presence of the filter. When the filter becomes wider, it increasingly fails to differentiate between frequencies. In the limit, all frequencies are fed back into the laser with exactly the same feedback strength. This corresponds to a situation where the envelope of the solution curve is given by the limiting Eq. (12). Figure 8 shows that indeed for a large filter width of $\Lambda = 2.0$ the solution curve and corresponding envelope are practically indistinguishable from those found for the ECMs of the COF laser. Finally, we note that, as $\Lambda \to \infty$, Eq. (6) reduces to

$$\Omega = \omega_s + \kappa\sqrt{1+\alpha^2}\sin(-C_p + \omega_s + \arctan(\alpha)).$$

This is the well-known transcendental equation defining the frequency of the ECMs in the COF laser; see, for example, [20].

We now consider the limit that the small filter width Λ goes to zero, so that the filter will only feed (light very near) a single frequency back into the laser. By this we mean that only a single maximum or minimum of the solution curve fits into the 'bulge' of the envelope. Physically, this can be quite well achieved when the filter width is below the line spacing of the laser, as is the case, for example, with reflections from a separate resonant Fabry-Perot cavity [1]. Due to the extreme frequency selectivity, the FOF system has the characteristics of an injected laser problem. However, the injected light obviously does not come from a separate master laser in this case. As a consequence the interpretation of the FOF parameters in terms of an injection problem is somewhat subtle.

An asymptotic analysis of the solution curve for narrow FOF is presented in Ref. [6]. The limiting cases of large and small Λ are also discussed in Ref. [13] in terms of the number of solutions that are possible. We concentrate here on the limits of the solution curve and the solution envelope, which are shown in Fig. 9 for $\Lambda = 0.0001$. Panels (a) to (c) are for detunings of $\Delta = 0.0$, 0.125 and 0.25, respectively. 'The bulge' of the envelope is now extremely narrow, located at $\omega_s = \Delta$. (Note that the width of the envelope in Fig. 9 has been exaggerated for clarity.) As can be seen from Fig. 9, indeed at most one extremum of the black solution curve 'fits' into the grey envelope. To find the limiting shape of the envelope we note that for $\omega_s = \Delta$ and $\Lambda = 0$, the equation for the envelope Eq. (11) reduces to $\Omega = \omega_s + \kappa\sqrt{1+\alpha^2}$. This defines the 'bulge' of Fig. 9 as a single 'peak' of width $\kappa\sqrt{1+\alpha^2}$. On the other hand, for $\omega_s \neq \Delta$ Eq. (11) reduces to $\Omega = \omega_s$. This gives the rest of the envelope as the diagonal line. Note that the envelope in Fig. 9 is indeed very close to this limit.

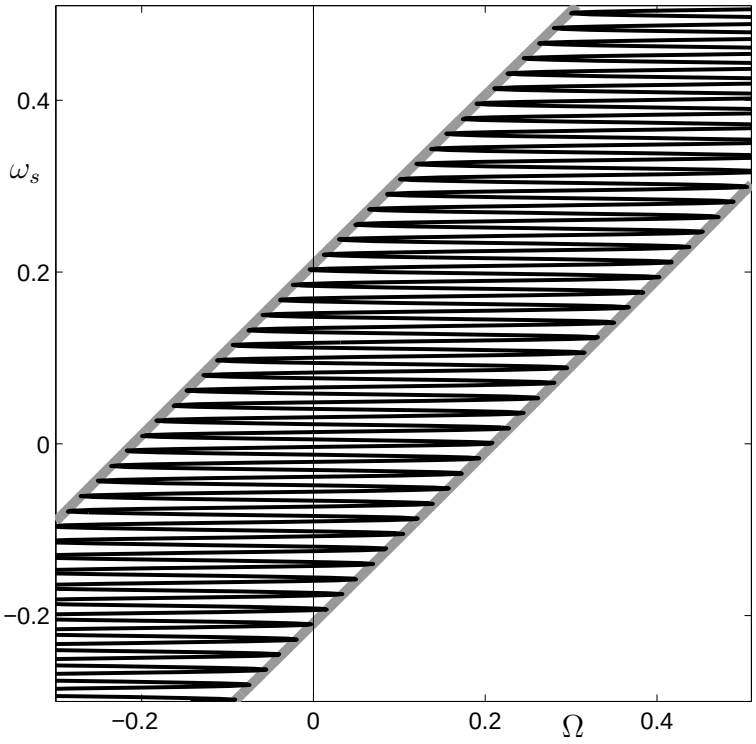

Fig. 8. COF limit of the FOF laser, shown for a large filter width of $\Lambda = 2.0$ ($\Delta = 0$).

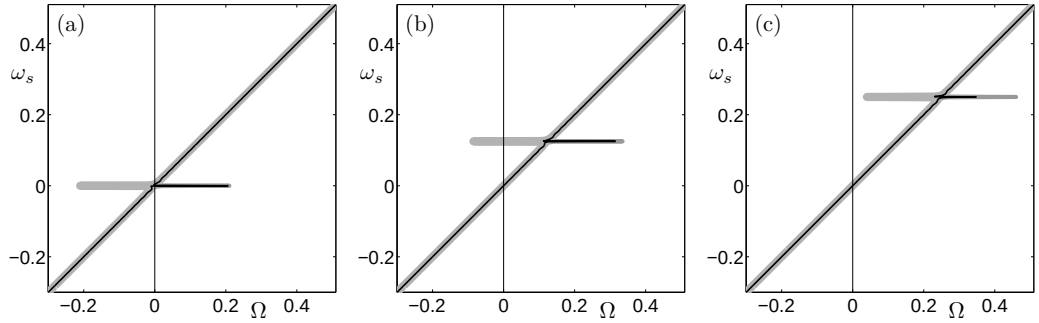

Fig. 9. Injection limit of the FOF laser, where a small filter width of $\Lambda = 1{\times}10^{-4}$ represents the injection limit. From (a) to (c) the filter detuning was fixed at $\Delta = 0.0$, 0.125, 0.25.

Recall that when changing C_p over 2π the envelope is filled out. In the limit the envelope does not leave much space for manoeuvre for the solution curve. In fact, the solution curve only has a single extremum in the bulge. It reaches the left extremum of the bulge for

$$C_p = \frac{\pi}{2} + \arctan\alpha + \Delta\tau + 2n\pi,\ n \in \mathbb{N}. \tag{20}$$

Likewise, it reaches the right extremum of the bulge for

$$C_p = \pi/2 + \arctan\alpha + \Delta\tau + (2n+1)\pi, \quad n \in \mathbb{N}.$$

These solutions are zeroes of the sine function of Eq. (6) for $\omega_s \to \Delta$ and $\Lambda = 0$. Between these values of C_p, the solution curve does not reach the extrema of the bulge of the envelope, as is the case in all panels of Fig. 9.

Finally, we note that in the injection laser the injection term appears in the equation of the electric field as $K_i e^{i\omega_i t}$, where K is the injection strength, and ω_i is the injection frequency. (See, for example, Refs. [23,24] for background reading on the injection laser.) In the limit of $\Lambda = 0$ we have that $\omega_i = \omega_s$, however the injection strength K_i depends on both the feedback rate κ, and the feedback phase C_p. Only for C_p satisfying Eq. (20) do we have that $K = \kappa$; see also Ref. [13].

5 Conclusions

We have performed an analysis of the EFM structure of the FOF laser in dependence on the key parameters of filter width Λ, filter detuning Δ, effective feedback strength $\kappa\sqrt{1+\alpha^2}$ and feedback phase C_p. Specifically, we found analytic expressions for both the solution curves, which define the frequency and amplitude of the EFMs, and the solution envelopes which bound these curves. This allowed us to show how the (Λ, Δ)-plane is divided into regions with either one or two EFM-components. The boundary between these regions is given by transitions through extrema and saddles (in the surface of EFMs). Finally, we briefly investigated the large and small Λ limits of the FOF laser, which can be identified as the COF and the injected laser, respectively.

We took the view that the laser remains at a fixed free-running frequency during an experiment, which has advantages in terms of the resulting formulas. Our results can readily be interpreted in the case that one keeps the filter frequency fixed and instead changes the free-running laser frequency to effect a detuning.

The EFM structure presented here forms the 'backbone' of the dynamics of the FOF laser. The next logical step is to perform a stability analysis of the EFMs, detect Hopf bifurcations and find and follow the bifurcating periodic solutions, possibly all the way to transitions to chaotic dynamics. This is a topic for future research, as already the analytical determination of the EFMs' stability is very challenging. Numerical continuation techniques will play an important role in unravelling the overall dynamics of the FOF laser, because they allow one to find and follow EFMs and periodic orbits while monitoring their stability to find bifurcations.

Acknowledgements

We acknowledge fruitful discussions with Hartmut Erzgräber, Daan Lenstra, Mirvais Yousefi, Matthias Wolfrum and Hans-Jürgen Wünsche. The research of B.K. is supported by an Advanced Research Fellowship from the Engineering and Physical Sciences Research Council (EPSRC).

Appendix

The rate equations for FOF from a single Lorentzian filter for the electric field A, the inversion Z and the feedback X are given as [26,28]:

$$\frac{dA}{dt'} = \frac{1}{2}(1+i\alpha)\xi Z(t')A(t') + \gamma X(t'), \tag{21}$$

$$\frac{dZ}{dt'} = -\beta Z(t') - (\Gamma_0 + \xi Z(t'))(|A(t')|^2 - P_0) \tag{22}$$

$$\frac{dX}{dt'} = \lambda A(t'-\theta)e^{i(\phi-\Omega_{\rm ref})} + (i(\Omega_m - \Omega_{\rm ref}) - \lambda)X(t'), \tag{23}$$

where

$$\beta = \frac{1+\xi T_1 P_0}{T_1}, \quad P_0 = \frac{J - J_{\rm th}}{\Gamma_0}. \tag{24}$$

Furthermore, the current density or pump rate $J = 1.5J_{\rm th} = 1.5Z_{\rm th}/T_1 = 1.4\times10^{17}$ s^{-1}. The values of the physical parameters are given in Refs. [26,28] as the linewidth enhancement factor $\alpha = 5$, the differential gain $\xi = 2142$ s^{-1}, the carrier lifetime $T_1 = 1.1\times10^{-9}$ s, the inversion at threshold $Z_{\rm th} = 1.5417\times 10^8$ s, the photon decay rate $\Gamma_0 = 3.57\times10^{11}$ s^{-1}, the feedback rate $\gamma = 14.71$ Hz, and the propagation time between the laser and the external reflector $\theta = 1\times10^9$ s. Other, variable parameters include the filter width λ, and the filter detuning Ω_m.

Equations (21)–(23) can be simplified and the number of parameters reduced as follows. By introducing the rescaled electric field E, inversion N, feedback F and time t by

$$E = \sqrt{\frac{\xi T_1}{2}}A, \quad N = \frac{\xi}{2\Gamma_0}Z, \quad F = \sqrt{\frac{\xi T_1}{2}}X, \quad t' = \frac{t}{\Gamma_0} \tag{25}$$

giving Eqs. (1)–(3); see Sec. 2. The dimensionless parameters are related to the physical parameters as follows:

$$\kappa = \frac{\gamma}{\Gamma_0}, \quad T = T_1\Gamma_0, \quad P = \frac{\xi T_1}{2\Gamma_0}(J - J_{\rm th}), \quad \Lambda = \frac{\lambda}{\Gamma_0}, \quad \tau = \frac{\theta}{\Gamma_0},$$
$$\Delta = \frac{\Omega_m}{\Gamma_0}, \quad C_p = \frac{\phi}{\Gamma_0}, \quad \Omega = \frac{\Omega_{\rm ref}}{\Gamma_0}. \tag{26}$$

For the parameters given above we have $\kappa = 4.12045 \times 10^{-2}$, $T = 392.7$, $P = 0.185$, $\tau = 357$, and $\alpha = 5$.

References

[1] B. Dahmani, L. Hollberg, and R. Drullinger. Frequency stabilization of semiconductor lasers by resonant optical feedback. *Optics Lett.*, 12(11):876–878, 1987.

[2] D. H. DeTienne, G. R. Gray, G. P. Agrawal, and D. Lenstra. Semiconductor laser dynamics for feedback from a finite-penetration-depth phase-conjugate mirror. *IEEE J. Quantum Electron.*, 33:838–844, 1997.

[3] O. Diekmann, S. A. Van Gils, S. M. Verduyn Lunel, and H. O. Walther. *Delay Equations: Functional-, Complex-, and Nonlinear Analysis*, volume 110. Springer-Verlag, 1995.

[4] E. Doedel, A. Champneys, T. Fairgrieve, Yu. Kuznetsov, B. Sandstede, and X. Wang. AUTO 97: Continuation and bifurcation software for ordinary differential equations, 1997. `http://indy.cs.concordia.ca/auto/main.html`.

[5] K. Engelborghs, T. Luzyanina, and G. Samaey. DDE-BIFTOOL v2.00: a Matlab package for bifurcation analysis of delay differential equations. Technical Report TW-330, Department of Computer Science, K. U. Leuven, Belgium, 2001. `http://www.cs.kuleuven.ac.be/~koen/delay/ddebiftool.shtml`.

[6] T. Erneux, G. Hek, M. Yousefi, and D. Lenstra. The injection laser limit of lasers subject to optical feedback. In D. Lenstra, editor, *Semiconductor Lasers and Laser Dynamics*, volume 5452 of *Proceedings of SPIE*, pages 303–311, 2004.

[7] A. P. A. Fischer, O. K. Anderson, M. Yousefi, S. Stolte, and D. Lenstra. Experimental and theoretical study of filtered optical feedback in a semiconductor laser. *IEEE J. Quantum. Elec.*, 36(3):375–384, 2000.

[8] A. P. A. Fischer, M. Yousefi, D. Lenstra, M. W. Carter, and G. Vemuri. Filtered optical feedback induced frequency dynamics in semiconductor lasers. *Phys. Rev. Lett.*, 92(2):023901(1–4), 2004.

[9] K. Green and B. Krauskopf. Bifurcation analysis of frequency locking in a semiconductor laser with phase-conjugate feedback. *Int. J. Bif. Chaos*, 13(9):2589–2601, 2003.

[10] K. Green and B. Krauskopf. Bifurcation analysis of a semiconductor laser subject to non-instantaneous phase-conjugate feedback. *Opt. Commun.*, 231:383–393, 2004.

[11] J. K. Hale and S. M. Verduyn Lunel. *Introduction to Functional Differential Equations*. Springer-Verlag, 1993.

[12] T. Heil, I. Fischer, W. Elsäßer, B. Krauskopf, K. Green, and A. Gavrielides. Delay dynamics of semiconductor lasers with short external cavities: Bifurcation scenarios and mechanisms. *Phys. Rev. E*, 67(066214), 2003.

[13] G. Hek and V. Rottschäfer. Semiconductor laser with filtered optical feedback: bridge between conventional feedback and optical injection. In *Proc. 5th EUROMECH Nonl. Dyn. Conf.*, 2005.

[14] S. Jin, Y. Li, and M. Xiao. Single-mode diode laser with a large frequency-scanning range based on weak grating feedback. *Applied Optics*, 35(9):1436–1441, 1996.

[15] B. Krauskopf. *Unlocking Dynamical Diversity: Optical Feedback Effects on Semiconductor Lasers*, chapter 5 Bifurcation Analysis of Lasers with Delay. Wiley, March 2005.

[16] B. Krauskopf and D. Lenstra, editors. *Fundamental Issues of Nonlinear Laser Dynamics*, volume 548. AIP Conf. Proc., 2000.

[17] B. Krauskopf, G. H. M. Van Tartwijk, and G. R. Gray. Symmetry properties of lasers subject to optical feedback. *Opt. Commun.*, 177:347–353, 2000.

[18] R. Lang and K. Kobayashi. External optical feedback effects on semiconductor injection laser properties. *IEEE J. Quantum Electron.*, 16(3):347–355, 1980.

[19] D. Lenstra, G. Vemuri, and M. Yousefi. *Unlocking Dynamical Diversity: Optical Feedback Effects on Semiconductor Lasers*, chapter 4 Generalized Optical Feedback: Theory. Wiley, March 2005.

[20] D. Lenstra and M. Yousefi. Theory of delayed optical feedback in lasers. In Krauskopf and Lenstra [16], pages 87–111.

[21] H. Preir. Physics and applications of IV–VI compound semiconductor lasers. *Semicond. Sci. Technol.*, 5:S12–S20, 1990.

[22] G. H. M. Van Tartwijk and A. M. Levine. Sisyphus effect in semiconductor lasers with optical feedback. *IEEE J. Quantum. Elec.*, 1(2):466–472, 1995.

[23] S. Wieczorek, B. Krauskopf, and D. Lenstra. A unifying view of bifurcations in a semiconductor laser subject to optical injection. *Opt. Commun.*, 172:279–295, 1999.

[24] S.M. Wieczorek, B. Krauskopf, T.B. Simpson, and D. Lenstra. The dynamical complexity of optically injected semiconductor lasers. *Physics Reports*, 2005; to appear.

[25] H. Yasaka and H. Kawaguchi. Linewidth reduction and optical frequency stabilization of a distributed feedback laser by incoherent optical negative feedback. *Appl. Phys. Lett.*, 53(15):1360–1362, 1988.

[26] M. Yousefi. *On the dynamics of coupled semiconductor lasers*. PhD thesis, Vrije Universiteit te Amsterdam, 2003.

[27] M. Yousefi and D. Lenstra. Dynamical behavior of a semiconductor laser with filtered external feedback. *IEEE J. Quantum Electron.*, 35(6):970–976, 1999.

[28] M. Yousefi, D. Lenstra, and G. Vemuri. Nonlinear dynamics of a semiconductor laser with filtered optical feedback and the influence of noise. *Phys. Rev. E*, 67(046213), 2003.